Numerical modeling of mode-locked fiber lasers with a fiber-based saturable-absorber

Article *in* Optics Communications · January 2017

DOI: 10.1016/j.optcom.2016.09.035

CITATIONS
6

READS
633

3 authors, including:

Andy Chong
University of Dayton
103 PUBLICATIONS **4,566** CITATIONS
SEE PROFILE

Joseph W Haus
University of Dayton
446 PUBLICATIONS **8,364** CITATIONS
SEE PROFILE

Optics Communications 383 (2017) 386–390

Contents lists available at ScienceDirect

Optics Communications

journal homepage: www.elsevier.com/locate/optcom

Numerical modeling of mode-locked fiber lasers with a fiber-based saturable-absorber

Long Wang [a], Andy Chong [a,b], Joseph W. Haus [a,b,*]

[a] Department of Electro-optics and Photonics, University of Dayton, 300 College Park, Dayton OH 45469, USA
[b] Physics Department, University of Dayton, 300 College Park, Dayton, OH 45469 USA

ARTICLE INFO

Article history:
Received 12 August 2016
Accepted 16 September 2016
Available online 22 September 2016

Keywords:
Nonlinear optical fibers
Mode-locked fiber laser
Saturable absorber

ABSTRACT

We report fiber laser simulations with a fiber compatible, self-focusing, saturable absorber (SA) device. The SA device consists of two tapered fiber ends separated by a bulk, nonlinear medium. An optical beam transmitted from one tapered fiber end, propagate through the nonlinear medium (chalcogenide glass $As_{40}Se_{60}$) and couples back into the other tapered fiber end. Pulse propagation in the fiber laser cavity is performed using the Split Step Method. Stable pulses are generated with energies around 0.3 nJ and a transform limited pulse width around 200 *fs*.

1. Introduction

A saturable absorber (SA) device is placed in a laser cavity to suppress continuous wave operation and to promote cooperation between many modes to sustain ultrashort pulse operation. A saturable absorber imparts losses to pulses within the cavity. The losses are relatively large at low intensities, but are significantly smaller for higher intensities. A pulse becomes shorter in time after passing through the SA, since the high intensity at the peak of the pulse saturates the absorber more strongly than its low intensity wings. Even in the presence of SAs the pulses can grow from intensity noise fluctuations in the cavity to achieve self-starting mode locking action.

Various SA mechanisms have been proposed to achieve the desired range intensity discrimination. Current commercial ultrafast lasers generally use semiconductor saturable absorber mirrors (SESAMs) [1,2]. Due to the well-established nanofabrication technology, they provide good control of the critical SA parameters, i.e. modulation depth, non-saturable loss and saturation power. However, due to the use of highly complex equipment in the fabrication process, a SESAM is generally pricy and bulky, which are not desirable characteristics for devices in fiber laser cavities. Other SA examples, based on a material nonlinearity, include: carbon based absorbers such as single-walled carbon nanotubes (SWCNTs) [3], graphene based absorbers [4] and so on. All these SAs have technical drawbacks. For example, CNTs generally suffer high non-saturable losses and graphene based absorbers have low modulation depth [5].

The disadvantages of the SAs mentioned above have spurred scientists' interest to develop artificial SAs based on nonlinear effects. These efforts give rise to the Kerr lens mode locking based on Optical Kerr effect [6] and nonlinear polarization evolution (NPE) based on the nonlinear effect in fibers [7,8]. Fiber lasers with NPE are inherently environmentally unstable and subtle fiber distortions can result in different output pulses from the same cavity. Furthermore, NPE effect is not accessible in cavities where polarization maintaining (PM) fibers are used. In contrast, Kerr lens mode locking based on optical Kerr effect is also suitable where PM fibers are needed.

Kerr lens mode locking was first reported for Ti: sapphire lasers in 1991 by Spence's group [9] and achieved pulses as short as 60 fs pulses. The reason ultra-short pulses can be generated with Kerr effect is due to the ultrafast response time of the electronic effect, which has enabled the generation of the shortest pulses with pulse width of ~5 fs [10]. The realization of Kerr lens mode locking action involves using the third order nonlinearity in conjunction with a hard (soft) aperture and has not been used in a fiber laser cavity. We recently report a new fiber-based saturable absorber design based on focusing the Kerr Effect [11]. The new SA design has two tapered fiber ends separated by a space with a nonlinear Kerr medium between them. The SA characteristics of the device were calculated using carbon disulfide ($\mathbf{CS}_2$) and chalcogenide glass $\mathbf{As}_2\boldsymbol{S}_3$ as the nonlinear medium [11]. The materials were chosen because of their large Kerr nonlinearity. As shown in Ref. ([11]), the new proposed SA design enjoys high modulation depth, ultrafast response time and has very low manufacturing cost. In this paper, we replace the nonlinear medium by another type of chalcogenide glass $\mathbf{As}_{40}\boldsymbol{Se}_{60}$ and calculate the SA action following the same procedure as in [11]. Once SA action is obtained, we investigate its pulse shaping performance in a fiber

* Corresponding author at: Department of Electro-optics and Photonics, University of Dayton, 300 College Park, Dayton, OH 45469, USA.
E-mail address: JHaus1@udayton.edu (J.W. Haus).

http://dx.doi.org/10.1016/j.optcom.2016.09.035
0030-4018/

laser cavity using standard simulation technique – split step method.

2. Saturable absorber action with $As_{40}Se_{60}$

As shown in reference [11] (see Fig. 2 in [11]), the SA action of the proposed design is a function of the beam sizes at the fiber ends, nonlinear coefficient and the thickness of the nonlinear medium (D). In this paper, we assume both the transmitting and receiving fibers are tapered from a normal single mode fiber, which has an outer diameter of 125 μm and core diameter of 8.2 μm. The fibers are tapered to have an outer diameter of 40 μm, which has the largest mode radius among different tapered fibers which in turn effectively reduces the need for high nonlinearity. The gap between fiber ends is D=3 mm and is filled with a plate of chalcogenide glass $As_{40}Se_{60}$. At tele-communication wavelength of $1.55\mu m$, $As_{40}Se_{60}$ has been found to have both high nonlinearity and figure of merit {FOM[$=n_2/\beta\lambda$, with β the two photon absorption coefficient]}, $2.3\times10^{-17}m^2/W$ and 11, respectively [12,13]. It is worth to mentioning that extremely large third order nonlinearity, including material ablation, has been reported near $1\mu m$; $9.0\pm1.4\times10^{-16}m^2/W$ using a $4.8\mu m$ thick $Te_{20}As_{30}Se_{50}$ thin film [14] at $1064nm$. Published values of n_2 vary from 2000 to 27000 times larger than n_2 values for fused silica ($n_{2\_fused\_silica}=3.0\times10^{-20}m^2/W$) at $1.05\mu m$ in Ag doped $As_{40}Se_{60}$ [15]. Specially in [15], higher dopant of silver generally results in higher nonlinearity. However, high percentage of dopant of silver inevitably increases the linear absorption rate.

For our simulations we apply the reported values from Reference [12]; the nonlinear index and the refractive index for $As_{40}Se_{60}$ at $\lambda=1.55\mu m$ are $n_2=2.3\times10^{-17}m^2/W$ and $n_0=2.81$, respectively. The corresponding critical power for self-focusing an optical beam is given by the following estimated expression [16,17]:

$$P_{cr}=0.148\frac{\lambda^2}{n_0 n_2}=5.43kW, \quad (1)$$

where n_0 is the refractive index, λ is the vacuum wavelength and n_2 is the Kerr nonlinearity, as given above.

Following the same procedure in [11], one can calculate the SA action for the proposed SA device, which is plotted in Fig. 1. In this paper, all the powers used are taken to be smaller than the critical power, since beyond the critical power the beam becomes unstable and collapse to a filament can occur [18].

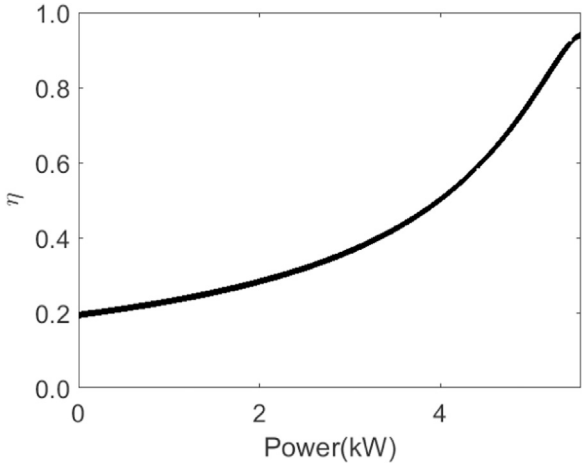

Fig. 1. Transmission (η) for ChG $As_{40}Se_{60}$ fiber-based SA at $D=3mm$. See Reference [11] for details about the calculations.

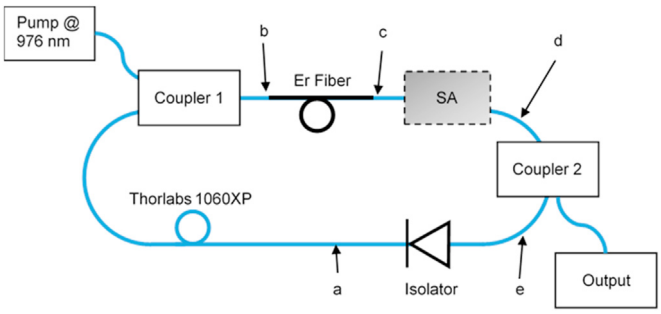

Fig. 2. Conceptual fiber laser cavity with the new saturable absorber design. Coupler1 transmits wavelengths near 976 nm, which co-propagate with the 1550 nm wavelength. Coupler 2 splits the input into two parts: one passes to the output port and the other couples the pulse back into the fiber cavity. In the fiber cavity, the black fiber is the Er-doped gain fiber and the blue fiber parameters use data for the Thorlabs 1060XP. Point *a* is chosen at the beginning of the PF, *b* at the beginning of the AF, *c* before the SA, *d* before the output coupler and *e* after the output coupler. An isolator is used to ensure that the pulse is propagating clockwise. Pigtails for couplers and the isolator are assumed to be short and ignored in our simulations. (For interpretation of the references to color in this figure legend, the reader is referred to the web version of this article.)

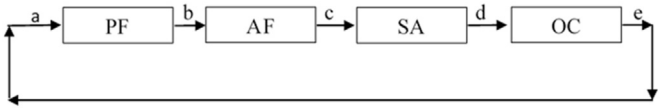

Fig. 3. Effective laser cavity for the simulation. PF=passive fiber, AF=active fiber, SA=saturable absorber, and OC=output coupler.

Table 1
Polynomial coefficients of SA action for $As_{40}Se_{60}$.

Coefficient	$As_{40}Se_{60}$
c_4	5.4223×10^{-4}
c_3	8.3644×10^{-5}
c_2	9.70522×10^{-4}
c_1	0.038705
c_0	0.1922079

Table 2
Simulation details.

Passive Fiber	$length L_{pf}(cm)$	600
	$\beta_2(ps^2/cm)$	-9.77×10^{-5}
(***Thorlabs 1060XP***)	$\gamma(1/cm\_W)$	1.3×10^{-5}
	$\alpha(1/cm)$	0
Gain Fiber	$length L_{af}(cm)$	55
	$\beta_2(ps^2/cm)$	16.5×10^{-5}
	$\gamma(1/cm\_W)$	2.8×10^{-5}
	$\alpha(1/cm)$	0
(***Thorlabs Er30 4/125***)	$g_0(1/cm)$	0.069077
	$\Delta\lambda(nm)$	40
	$E_{sat}(nJ)$	1.4
OC	R	0.8 or 0.7
Initial Pulse	$T_{max}(ps)$	120
	n_t	2^{14}
	$P_0(W)$	1
	$F_0(ps)$	1
	m_0	1
	C_0	0

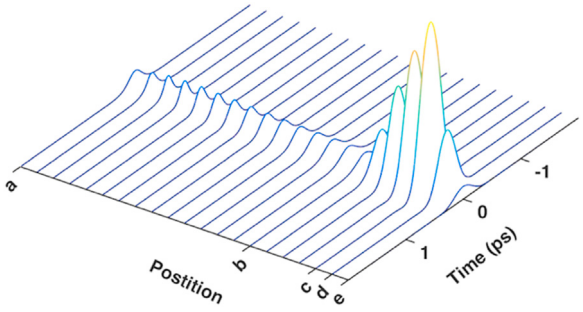

Fig. 4. Snapshots of stable pulse evolution inside the cavity. The axis labeled 'Position' follows the pulse evolution in the cavity. The starting point is at the beginning of the PF (see Fig. 3). The rest of the labels are marked in Fig. 3 and stand for the ending point of the previous element. z axis is the pulse power, which is normalized to the peak power inside the cavity and not shown for simplicity. $R = 0.8$.

3. Setup of laser cavity and numerical model

The general conceptual laser cavity under study is shown in Fig. 2. The gain fiber under simulation is Erbium doped, which is based on Thorlabs Er30 4/125 and passive fibers are Thorlabs 1060XP. Pump light is coupled into the cavity through coupler 1 and pulses are coupled out of the cavity through coupler 2. An isolator is used to ensure pulses are propagating in one direction. The SA action is incorporated into the simulation using results from the previous section. Fiber leads to the couplers and isolator are assumed to be short and ignored. Thus the cavity effectively consist of four elements: a passive fiber (PF), an active fiber (AF), a saturable absorber (SA) and an output coupler (OC), schematically shown in Fig. 3.

The pulse simulation in fibers is governed by the generalized nonlinear Schrodinger equation (NLSE) [19]. Self-steepening and intra-pulse Raman scattering can be ignored since the pulses from our study are relatively broad, which minimizes the contributions from those processes. Considering only second order fiber dispersion, we rewrite the pulse propagation equation in a fiber as

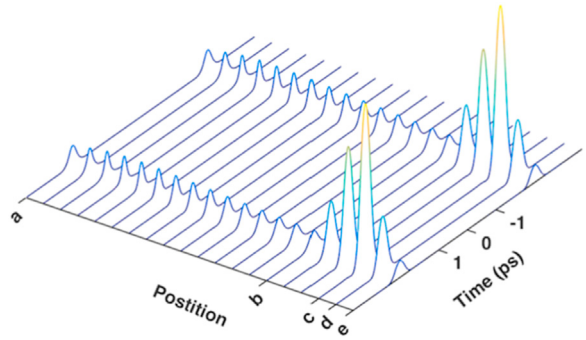

Fig. 6. Snapshots of stable pulse evolution inside the cavity as shown in Tables 2, R=0.7. z axis is the pulse power, which is normalized to the peak power inside the cavity and not shown for simplicity.

$$\frac{\partial A}{\partial z} = \frac{\hat{g}}{2}A - \frac{\alpha}{2}A - i\frac{\beta_2}{2}\frac{\partial^2 A}{\partial T^2} + i\gamma|A|^2A, \tag{2}$$

where A is the slowly varying amplitude of the pulse envelope, z the propagation coordinate, and T the retarded time. β_2 is the group velocity dispersion (GVD); γ is the nonlinearity parameter given by $\gamma = n_2\omega_0/cA_{eff}$, where n_2 is the nonlinear index, ω_0 the central angular frequency, c the velocity of light in vacuum, and A_{eff} the effective mode area for the beam inside fiber. α is the linear fiber loss coefficient which is generally a small number and $\hat{g}$ the active time-dependent fiber gain function for active fibers. The gain function is evaluated in frequency space and is called the gain spectrum.

Gain spectrum in this work is assumed to have Gaussian shape centered at the pulse center wavelength, which is expressed in the following equation:

$$g(\omega) = \frac{g_0}{1+\frac{E(z)}{E_{sat}}} exp\left(-2.7726\left(\frac{\omega-\omega_0}{\Delta\omega}\right)^2\right), \tag{3}$$

where ω is the angular frequency, ω_0 the center angular frequency, $\Delta\omega$ the gain full-width-half- maximum (FWHM) bandwidth. g_0 is the small signal power gain. In this paper, we assume g_0=30dB/m.

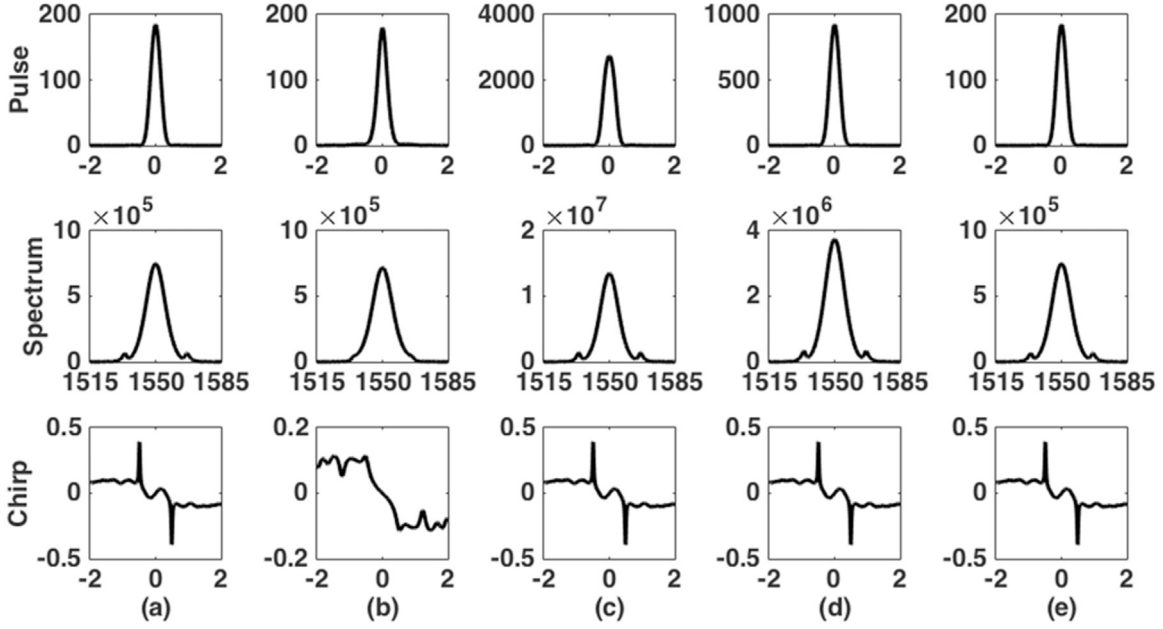

Fig. 5. Pulse evolution (top row, x axis in ps), corresponding spectrum (middle row, x axis in nm)) and chirp (bottom row, x axis in ps) inside the cavity at positions of (a) before the PF; (b) before the AF; (c) before the SA; (d). before the OC and (e) after the OC. The x axis for first and third row is in units of picoseconds and the second row in nm units. $R = 0.8$.

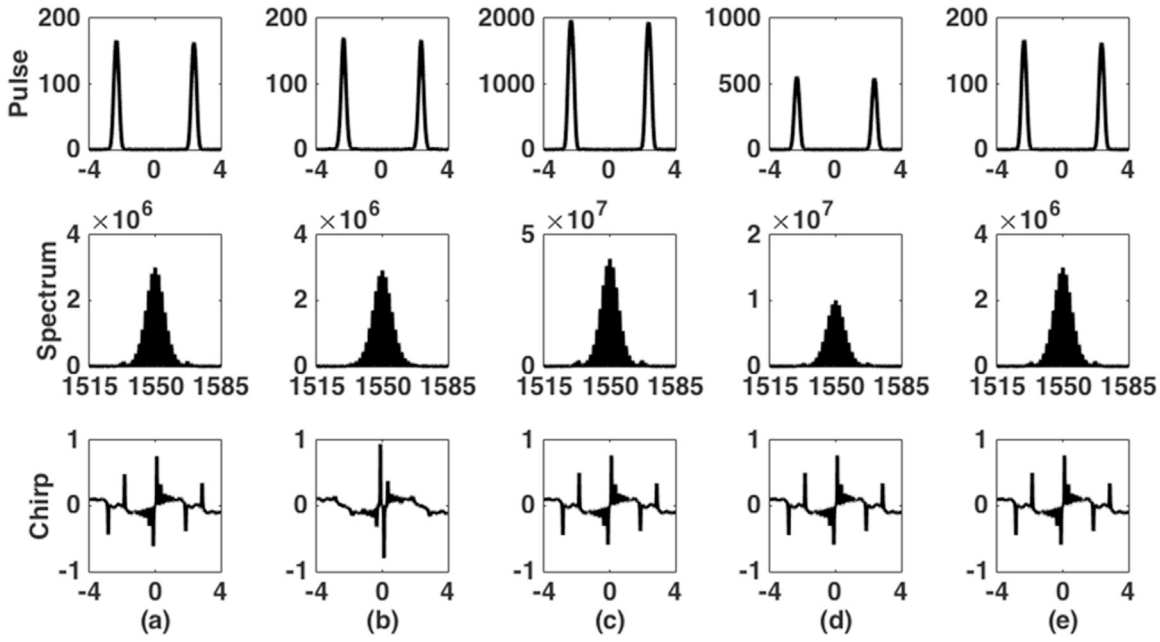

Fig. 7. Pulse evolution (top row), corresponding spectrum (middle row)) and chirp (bottom row) inside the cavity at positions of (a) before the PF; (b) before the AF; (c) before the SA; (d) before the OC and (e) after the OC. The x axis for first and third row is in units of picoseconds and the second row in nm units. The cavity corresponds to Table 2, R=0.7.

This number translates to a value of g_0=0.069077 cm^{-1}, using the relation in [19]. E_{sat}, the saturation energy, is the pulse energy of an incident pulse which leads to a reduction of the gain to e^{-1} of its small signal gain. Generally, the saturation energy E_{sat} depends on the wavelength, mode area, the overlap-inversion factor, absorption and emission cross-section, and so on. Exact treatment of such a value can be found in [20,21]. Since in the simulation we want to explore the potential output laser characteristics as functions of cavity design, saturation energy, as one of these parameters, can be adjusted numerically and adjustments to the simulation can be made for comparison with experiments. Usually we specify the FWHM wavelength bandwidth $\Delta\lambda$ using the relation $\Delta\omega = -\frac{2\pi c}{\lambda_0^2}\Delta\lambda$, where λ_0 is the center wavelength. $E(z)$ is the pulse energy $E=\int |A|^2 dT$. For passive fibers, the gain is simply set to be zero.

The SA device action in our simulation is modeled using a fourth order polynomial fit to the transmission data shown in Fig. 1. The transmission follows the format $\eta = c_4P^4 + c_3P^3 + c_2P^2 + c_1P^1 + c_0$, where the polynomial coefficients are shown in Table 1.

The output coupler is described by $A_{out} = \sqrt{R} * A_{in}$, here R is the power output coupling ratio.

An initial pulse is used as the starting point in simulations, which is assumed to follow a super-Gaussian profile:

$$A(t) = \sqrt{P_0} * e^{-\frac{1}{2}(1+iC_0)\left(\frac{t}{T_0}\right)^{2m_0}}, \quad (4)$$

where, P_0 is initial pulse power, C_0 the chirp, m_0 the beam shape factor and T_0 the pulse width. Several parameters are defined for the initial seed: full time window (T_{max}), number of data points (n_t), initial seed peak power (P_0), pulse full width half maximum duration (F_0), beam shape factor (m_0) and the chirp parameter (C_0). FWHM F_0 and T_0 are related by $T_0 = F_0/\left(2*\sqrt{\ln(2)}\right)$. Random noise is also used as the initial pulse and the exact treatment of such a quantity can be found in the Section 4.

Simulation details are summarized in Table 2.

4. Simulation results

The total cavity dispersion corresponding to Table 2 is −0. 049545ps^2 and the repetition rate is 31. 74MHz. The number of points used in our simulations is n_t. The parameters for the initial pulse in Eq. (4) are also found in Table 2 (R = 0. 8). The stable pulse inside the laser cavity is shown in Fig. 4, with particular positions labeled according to the Figs. 2 and 3. Inside the passive fiber (from a to b), the pulse is initially compressed. But by the end of PF excess dispersion leads to pulse broadening. Entering into the gain fiber (from b to c), the pulse is amplified and the spectrum is broader, which are then compensated by the SA (from c to d) and OC (from d to e). The pulses at each specified position are plotted in Fig. 5, where the top row is the pulse intensity profile, middle row is the spectrum of the pulse, and the bottom row is the corresponding chirp. The output pulse energy is about 0. 2731nJ and the calculated transform limited pulse has a power full-width-half-maximum ~200fs. However, as shown, the output pulses have a complex chirp structure and it would be challenging to dechirp the pulses close to the transform limited ones.

Gaussian noise is added into the initial Gaussian input as described in Table 2. Specifically, the noisy Gaussian input takes either the form of $\sqrt{P_0}\left[\mathrm{NL}*\mathrm{randn}(1,\mathrm{nt})+\exp\left(-0.5*\left(\frac{t}{T_0}\right)^2\right)\right]$ or $\sqrt{P_0}\left[\mathrm{NL}*\mathrm{rand}(1,\mathrm{nt})+\exp\left(-0.5*\left(\frac{t}{T_0}\right)^2\right)\right]$, where NL (noise level) is tuned from 0 to 1. Despite the different noises, the pulses always converge to the same solution, which demonstrates that the pulse set shown in Figs. 4 and 5 is a true attractor to the cavity described in Table 2.

Other cavities have also been explored with the proposed SA action. Generally, higher active fiber gain (g_0) and longer active fiber length (L_{af}) produces pulses with higher energies. However, the SA action imposes the inherent limitation on the generation of higher energy pulses. Since pulses with peak power beyond the critical power of the proposed SA design will disrupt the pulse characteristics and thus this situation should be avoided. Starting from Table 2, different stable pulses can be generated by adjusting

the system parameters. All generated pulses demonstrate complex chirp structures and have output energies limited up to ~0. 32nJ (L_{pf}=700cm,L_{af}=60cm,g_0=0. 0652cm^{-1} with other parameters the same as in Table 2). The output coupling ratio also significantly affects the pulse generation. With a smaller output coupling ratios (R), the cavity shown in Table 2 tends to generate multi-pulses. Pulses for $R = 0.7$ are shown in Figs. 6 and 7 and the corresponding output pulse energy is ~0. 2919nJ.

5. Conclusion

In this paper we numerically study the pulse generation in a fiber laser cavity that incorporates a fiber-based Kerr lens SA device [11]. The proposed SA action device is the fiber analog of a Kerr lens SA by placing a nonlinear Kerr medium between two fiber ends. The Kerr lens device has been successfully inserted as a mode-locker in solid-state lasers and this device could be similarly used as a fiber-based mode-locker. The laser cavity in the simulations consists of a passive fiber, a gain fiber, the proposed SA design and an output coupler. Stable pulses are consistently generated with the output pulse energy around 0.29 nJ and a transform limited pulse width ~200 fs. However, as shown in the study, the pulses show complex chirp structures and it would be challenging to dechirp the pulses to the transform limited ones.

As previously explained, our proposed SA fiber devices enjoy many advantages over the other types of SA. For example, our SA fiber devices in a ring cavity are much more compact, compared to, say, nonlinear optical loop mirror and SESAM. It has a higher modulation depth, compared to graphene based absorbers. It does not modify the polarization state and could be used together with polarization rotation mode locking. However, since our SA devices are based on a nonlinear medium and could be destroyed if the pulse peak power goes beyond the critical power, total gain provided by the active fiber in our simulation are carefully controlled at a low level. By adjusting the system parameters, pulses with energy up to ~0.32 nJ are obtained and the corresponding total small signal power gain from the active fiber is 18 dB. By stretching the pulses sufficiently before entering into the SA device, it would be possible to generate pulses with even higher energies; further numerical studies should be conducted to optimize the cavity for the purpose of designing fiber laser experiments.

References

[1] U. Keller, Recent developments in compact ultrafast lasers, Nature 424 (2003) 831–838.
[2] U. Keller, K.J. Weingarten, F.X. Kärtner, D. Kopf, B. Braun, I.D. Jung, R. Fluck, C. Hönninger, N. Matuschek, J. Aus Der Au, Semiconductor saturable absorber mirrors (SESAM's) for femtosecond to nanosecond pulse generation in solid-state lasers, IEEE J. Sel. Top. Quantum Electron. 2 (1996) 435–451.
[3] I.H. Baek, S.Y. Choi, H.W. Lee, W.B. Cho, V. Petrov, A. Agnesi, V. Pasiskevicius, D.-I. Yeom, K. Kim, F. Rotermund, Single-walled carbon nanotube saturable absorber assisted high-power mode-locking of a Ti: sapphire laser, Opt. Express 19 (2011) 7833–7838.
[4] M.N. Cizmeciyan, J.W. Kim, S. Bae, B.H. Hong, F. Rotermund, A. Sennaroglu, Graphene mode-locked femtosecond Cr: ZnSe laser at 2500 nm, Opt. Lett. 38 (2013) 341–343.
[5] A. Martinez, Z. Sun, Nanotube and graphene saturable absorbers for fibre lasers, Nat. Photonics 7 (2013) 842–845.
[6] T. Brabec, C. Spielmann, P.F. Curley, F. Krausz, Kerr lens mode locking, Opt. Lett. 17 (1992) 1292–1294.
[7] V.J. Matsas, D.J. Richardson, T.P. Newson, D.N. Payne, Characterization of a self-starting, passively mode-locked fiber ring laser that exploits nonlinear polarization evolution, Opt. Lett. 18 (1993) 358–360.
[8] K. Tamura, H.A. Haus, E.P. Ippen, Self-starting additive pulse mode-locked erbium fibre ring laser, Electron. Lett. 28 (1992) 2226.
[9] D.E. Spence, P.N. Kean, W. Sibbett, 60-fsec pulse generation from a self-mode-locked Ti: sapphire laser, Opt. Lett. 16 (1991) 42–44.
[10] R. Ell, U. Morgner, F.X. Kärtner, J.G. Fujimoto, E.P. Ippen, V. Scheuer, G. Angelow, T. Tschudi, M.J. Lederer, a Boiko, B. Luther-Davies, Generation of 5-fs pulses and octave-spanning spectra directly from a Ti: sapphire laser, Opt. Lett. 26 (2001) 373–375.
[11] L. Wang, J.W. Haus, Fiber-based saturable-absorber action based on a focusing Kerr effect, Opt. Commun. 367 (2016) 292–298.
[12] J.M. Harbold, F.O. Ilday, F.W. Wise, J.S. Sanghera, V.Q. Nguyen, L.B. Shaw, I. D. Aggarwal, Highly nonlinear As-S-Se glasses for all-optical switching, Opt. Lett. 27 (2002) 119–121.
[13] J.S. Sanghera, C.M. Florea, L.B. Shaw, P. Pureza, V.Q. Nguyen, M. Bashkansky, Z. Dutton, I.D. Aggarwal, Non-linear properties of chalcogenide glasses and fibers, J. Non Cryst. Solids 354 (2008) 462–467.
[14] K. Fedus, G. Boudebs, C.B. De Araújo, M. Cathelinaud, F. Charpentier, V. Nazabal, Photoinduced effects in thin films of Te20 As30 Se50 glass with nonlinear characterization, Appl. Phys. Lett. 94 (2009) 061122.
[15] K. Ogusu, J. Yamasaki, S. Maeda, M. Kitao, M. Minakata, Linear and nonlinear optical properties of Ag-As-Se chalcogenide glasses for all-optical switching, Opt. Lett. 29 (2004) 265–267.
[16] G. Fibich, A.L. Gaeta, Critical power for self-focusing in bulk media and in hollow waveguides, Opt. Lett. 25 (2000) 335–337.
[17] R.W. Boyd, Nonlinear Optics, 3rd ed., Academic Press, San Diego, CA, 2008.
[18] A. Couairon, A. Mysyrowicz, Femtosecond filamentation in transparent media, Phys. Rep. 441 (2007) 47–189.
[19] G.P. Agrawal, Nonlinear Fiber Optics, 5th ed., Academic Press, San Diego, CA, 2006.
[20] E. Desurvire, Erbium-Doped Fiber Amplifiers: Principles and Applications, 1st ed., John Wiley & Sons, New York, 1994.
[21] F.I. Vasile, P. Schiopu, The determination of the saturation power for erbium doped fiber amplifier, J. Optoelectron. Adv. Mater. 6 (2004) 1207–1212.